Passive microfluidic pumping using coupled capillary/evaporation effects†

N. Scott Lynn and David S. Dandy*

Received 23rd June 2009, Accepted 25th August 2009
First published as an Advance Article on the web 5th October 2009
DOI: 10.1039/b912213c

Controlled pumping of fluids through microfluidic networks is a critical unit operation ubiquitous to lab-on-a-chip applications. Although there have been a number of studies involving the creation of passive flows within lab-on-a-chip devices, none has shown the ability to create temporally stable flows for periods longer than several minutes. Here a passive pumping approach is presented in which a large pressure differential arising from a small, curved meniscus situated along the bottom corners of an outlet reservoir serves to drive fluid through a microfluidic network. The system quickly reaches steady-state and is able to provide precise volumetric flow rates for periods lasting over an hour. A two-step mathematical model provides accurate predictions of fluid and mass transport dynamics in these devices, as validated by particle tracking in laboratory systems. Precise flow rates spanning an order of magnitude are accomplished *via* control of the microchannel and outlet reservoir dimensions. This flow mechanism has the potential to be applied to many micro-total analytical system devices that utilize pressure-driven flow; as an illustrative example, the pumping technique is applied for the passive generation of temporally stable chemical gradients.

Introduction

Perhaps the most important unit operation within microfluidics based lab-on-a-chip (LOC) devices lies in the handling and transport of fluids. Often overlooked, the ability to provide continuous flow with high precision can dramatically improve the efficiency and reliability of devices utilizing the fundamentals of separation, reaction, and detection for bioanalytical purposes and point-of-care diagnostics.[1] These different processes are often carried out in a complex network of microchannels comprising a microfluidic network (μFN) that links the inlet/outlet regions serving as interfaces for analyte delivery or product and waste collection. The traditional mechanisms for fluid transport within μFNs rely on either pressure-driven flows from syringe pumps and pressurized chambers or flows derived from electrokinetic phenomena.[2,3] Although these active delivery methods are able to provide adjustable volumetric flow rates spanning multiple orders of magnitude, they possess a number of negative features including very large dead volumes, complicated sample–interface connections, and a minimum requirement of ~1 mL sized sample volumes. Furthermore, the utilization of these methods, along with less common flows based on centrifugal forces,[4] surface acoustic waves,[5] optical methods,[6] or micromechanical actuation,[7–9] generally requires equipment that is significantly larger in size than the μFN itself and can severely restrict device portability. Due to these limitations, there has been a significant amount of work focused on the creation of passive flows within μFNs. Demanding no external power input, passive flow methods require only fluid delivery to an inlet region (usually *via* pipette), after which filling of the μFN is spontaneous and the subsequent continuous flow is a function of the device design. Free from the size restrictions and power requirements of external equipment, LOC devices utilizing passive flow have great potential for use in point-of-care diagnostics and portable micro-total analysis systems.

Because of the inverse dependence of capillary pressure on the characteristic radius of curvature for an air/liquid interface, capillary forces are a convenient driving force for the creation of pressure-driven flow in hydrophilic microchannels. Passive flow from capillary forces in microchannels can be accomplished utilizing either static air/liquid menisci existing external to the μFN or menisci internal to the μFN whose positions move with time. Capillary pumps using internal menisci can be created *via* expanding channel networks in parallel such that the characteristic size of the outlet air/liquid meniscus remains of the order of the size of the microchannel.[10] These systems provide the ability to create very high differential pressures throughout the μFN and have been successfully applied to heterogeneous affinity assays, supplying near-constant continuous flow over the course of several minutes.[11,12] However, the pumping regions are ~1 cm^2 in size and must be enlarged to maintain continuous flow for longer periods of time.

By transferring the menisci responsible for the driving capillary force to a position external to the μFN, the overall footprint of a capillary pump can be reduced substantially. Passive capillary pumping has been demonstrated utilizing the difference in curvature for liquid drops placed on the inlet and outlet reservoirs of a μFN,[13] where the overall size of the pumping region is ~1 mm^2. Continuous flow between the reservoirs can be accurately described using simple analytical models accounting for the shape of each droplet;[14,15] however, these models do not account for liquid loss through evaporation. Because the combined effects of evaporation and convective flow from each

Department of Chemical and Biological Engineering, Colorado State University, Fort Collins, Colorado, 80523-1370, USA. E-mail: dandy@colostate.edu; Fax: +1 970 491 7369

† Electronic supplementary information (ESI) available: Summary of the model: including predictions of the meniscus shape, evaporation rate, and time-dependent flow in experimental systems utilizing this passive flow mechanism. See DOI: 10.1039/b912213c

reservoir will act to change the overall capillary forces present in the system, the flow is transient and can only be sustained for several minutes.[16] Additionally, prediction of flow rates within these droplet-based passive pumping systems may be problematic in situations where the position of the air/liquid meniscus drops below the top of the reservoir. In this case liquid volumes approach sub-μL quantities and the shape of the meniscus becomes sufficiently complicated such that the effects of evaporation cannot be determined using simplified models.

Although there exists a great deal of literature focusing on the kinematics of filling a μFN *via* capillary forces, where filling times are typically less than 100 s, few studies have focused on the creation of sustained continuous flows, and little to no data exist concerning the state of flow within a μFN after filling has completed. In the present work, a passive microfluidic pumping mechanism is demonstrated that combines the ability to create steady flows at high differential pressures within a mm^2 footprint. After sample introduction to an inlet reservoir, capillary forces drive fluid through a μFN spontaneously such that a small meniscus is created along the corner regions of an outlet reservoir (Fig. 1). The system quickly reaches steady-state and is able to provide constant flow rates through a μFN for more than an hour. Utilizing a simple model that accounts for both the rate of evaporation and the shape of an air/liquid interface for a given system,[17] accurate predictions of laboratory flow rates as a function of reservoir and μFN geometries are demonstrated. Only requiring the outlet microreservoir walls to be sufficiently hydrophilic, the passive pumping method described here stands alone in its ability to create steady flows for extended time periods, where the overall duration of flow is limited by the overall solute concentration and solubility. This simple approach may be applied to nearly all LOC devices utilizing pressure-driven flow; as an illustrative example, the pumping technique is applied for the passive generation of temporally stable chemical gradients.

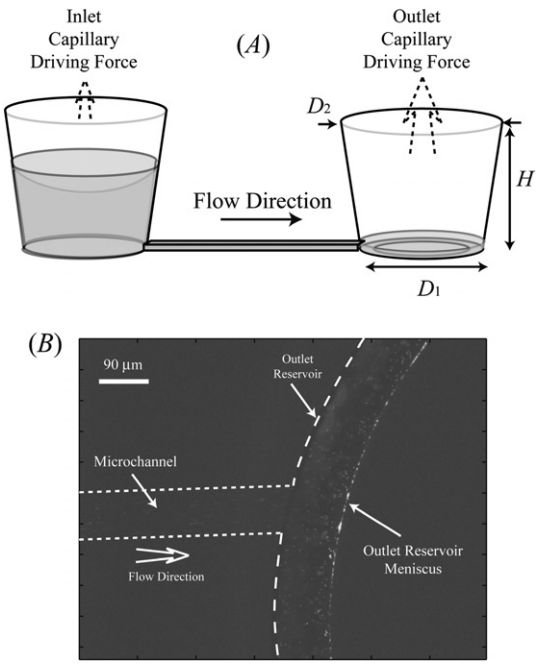

Fig. 1 (*A*) Diagram of overall system. The small meniscus along the corner regions of the outlet reservoir serves to drive fluid through a microchannel at high differential pressures. (*B*) Experimental image of 0.5 μm fluorescent tracer beads in a microchannel of width $w = 90$ μm, height $h = 28$ μm, and length $L = 20$ mm connected to an outlet reservoir with lower diameter $D_1 = 2.15$ mm, upper diameter $D_2 = 1.65$ mm, and height $H = 1.9$ mm. The position of the air/water interface along the reservoir floor does not move with time.

Results and discussion

Model

Upon introduction of an aqueous solution into the inlet reservoir, liquid spontaneously fills a hydrophilic microchannel and the corner regions of an outlet reservoir similar to the case shown in Fig. 1*A*, such that fluid moves between the reservoirs with a time-dependent volumetric flow rate Q_f. The laboratory systems used here are composed of polydimethylsiloxane (PDMS) microchannels and reservoirs bonded to a glass slide. It is important to develop a mathematical model to accurately predict $Q_f = Q_f(t)$ occurring in laboratory microchannels with height h, width w, and length L connecting reservoirs with height H, lower diameter D_1, and upper diameter D_2. In each reservoir the apparent contact angles between the aqueous solution and the reservoir floor and sidewalls are θ_1 and θ_2, respectively. For a liquid of density ρ and viscosity μ moving with average axial linear velocity $v = Q_f/wh$, typical Reynolds numbers ($Re = hv\rho/\mu$) in these μFNs are often smaller than 0.1 and flow is well within the laminar regime for all cases.

Via application of the Washburn equation, it is estimated that the time required for capillary forces to fill the μFNs relevant to this study is of the order of 1 s.[18] Wetting of the corner regions of the outlet reservoir (forming an incomplete meniscus) has been observed experimentally to be completed within 10 s. The cross-sectional view of an air/liquid interface within a reservoir can be seen in Fig. 2. Performing a mass balance on the liquid contents of a single reservoir yields

$$\frac{dV}{dt} = Q_f - Q_e - Q_{perm} \quad (1)$$

where $V(t)$ is the liquid volume present in the reservoir, Q_e is the loss due to evaporation from the air/liquid meniscus, Q_{perm} is the volumetric rate of permeation into the reservoir sidewalls, and Q_f

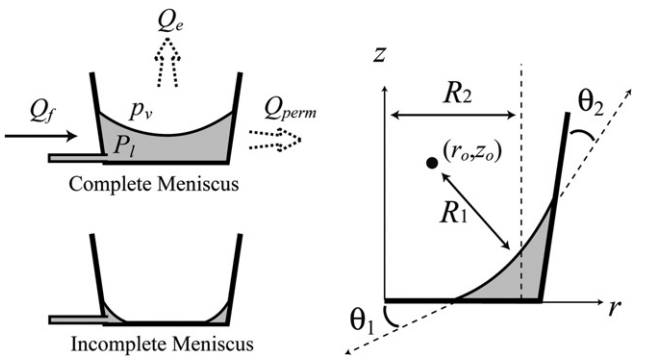

Fig. 2 Cross-sectional view of both a complete and an incomplete meniscus in a microreservoir. Geometric definitions for an incomplete meniscus shape are shown to the right.

is defined to be positive if fluid is moving into the reservoir. Because of the small characteristic length scales of the reservoirs the system may be assumed to be at pseudo-steady-state such that flow will respond nearly instantaneously to changes in the liquid volume present in either reservoir. The volumetric flow rate between the reservoirs can be determined from a flow resistance analogy as

$$Q_f = \frac{-\Delta p}{K} \tag{2}$$

where K is the viscous resistance to flow within the microchannel, $\Delta p = p_{l,out} - p_{l,in}$ is the differential fluid pressure between the two reservoirs, and the subscripts in and out denote the inlet and outlet reservoirs, respectively. Neglecting secondary effects due to the sudden contraction and expansion from the reservoir to the microchannel, the viscous resistance to laminar flow may be calculated as[19]

$$K = \frac{12\mu L}{w^3 h}\left[1 - \frac{192w}{\pi^5 h}\sum_{n=1,3,5,..}^{\infty}\frac{1}{n^5}\tan h\left(\frac{n\pi h}{2w}\right)\right]^{-1} \tag{3}$$

For quiescent liquid conditions the pressure differential Δp_i between the liquid and gas phase across a curved interface can be calculated using the Young–Laplace equation

$$\Delta p_i = p_v - p_l = \gamma\left(\frac{1}{R_1} + \frac{1}{R_2}\right) \tag{4}$$

where R_1 and R_2 are the two principal radii of curvature pertaining to the air/liquid meniscus, γ is the air/liquid interfacial tension, and the subscripts v and l indicate the vapor and liquid phase, respectively. For stable menisci existing within a microreservoir, R_1 and R_2 cannot be accurately measured with confocal or interference-contrast microscopy, nor can simple analytical solutions be derived such as those used in previous models.[14,15] However, using a geometric model to determine the shape of the meniscus in the reservoir, combined with computational fluid dynamics (CFD) simulations to predict the rate of evaporation from the meniscus, it is possible to accurately determine R_1, R_2, and Q_e given the defining parameters for a reservoir: D_1, D_2, H, T, RH (relative humidity), θ_1, θ_2, and V.[17] This accuracy of this model was verified in laboratory systems by observing the inner moving contact line for air/water menisci existing in a reservoir during liquid evaporation. Details of the model can be found within the ESI†.

Prediction of time-dependent flow

To validate the proposed flow model, the time-dependent average velocity v of 0.5 μm diameter fluorescent tracer beads was measured in PDMS/glass microchannels for an initial liquid volume V_o in the inlet reservoir. Predictions of $v(t)$ were obtained from the solution to eqn (1) using measured values of D_1, D_2, H, h, w, L, T, RH, θ_1, and θ_2 (*i.e.*, no adjustable parameters). Details of model implementation and analysis of data, along with laboratory observations of fluid flow near the microchannel outlet, may be found in the ESI†.

Fig. 3 displays both laboratory measurements and model predictions of the average fluid velocity as a function of time in microchannels (h = 28 μm, L = 20 mm) with different widths connecting expanding inlet/outlet reservoirs (D_1 = 2.15 mm, D_2 = 2.65 mm, H = 2.5 mm). Fig. 3*A* and *B* correspond to initial volumes V_o = 2.0 μL and 1.5 μL, respectively, placed in the inlet reservoir at t = 0. Although channels with larger w have lower steady fluid velocities, they possess larger values of both Q_f and $Q_{e,out}$; therefore both the time at which the inlet meniscus ruptures to an incomplete state (t_c) and the time at which the both reservoirs are empty (t_{end}) decrease with increasing w. Measured and predicted values of t_{end} were within 45 s of one another for all cases shown in Fig. 3.

As demonstrated in Fig. 3, the mathematical model of the passive flow mechanism described by eqn (1)–(4) accurately predicts the magnitudes of v as well as t_{end} for a variety of initial inlet liquid volumes and microchannel geometries. The small differences between experimental values and model predictions

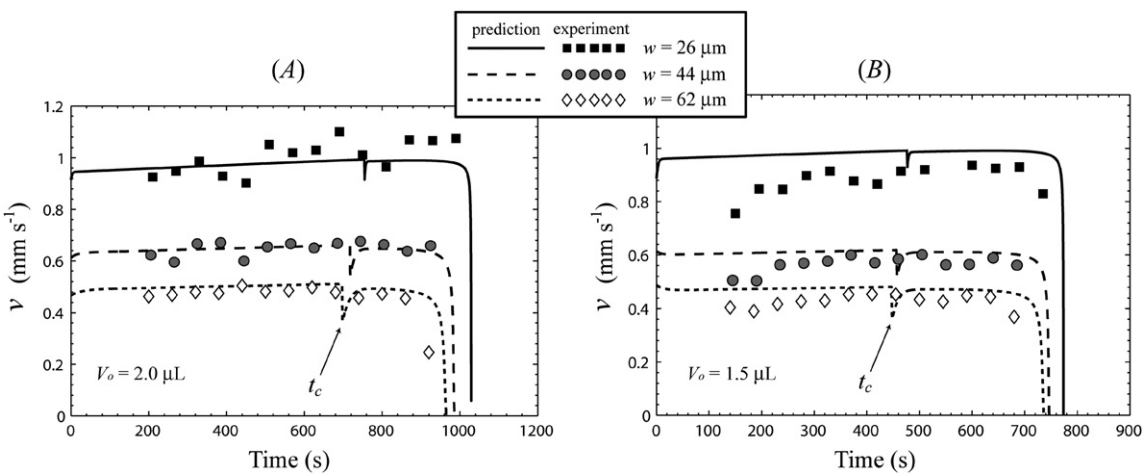

Fig. 3 Experimental and theoretical predictions of the average fluid velocity v as a function of time in microchannels with h = 28 μm, L = 20 mm, and varying width with reservoirs with dimensions D_1 = 2.15 mm, D_2 = 2.65, H = 2.5 mm and contact angles $\theta_{1,in}$ = 13°, $\theta_{2,in}$ = 49°, $\theta_{1,out}$ = 4.2°, and $\theta_{2,out}$ = 18.2°. (*A*) Initial inlet reservoir volume V_o = 2.0 μL. Experimental conditions were T_{begin} = 24.2 °C → T_{end} = 25.7 °C. RH_{begin} = 0.167 → RH_{end} = 0.177. (*B*) V_o = 1.5 μL with experimental conditions T_{begin} = 25.0 °C → T_{end} = 25.8 °C. RH_{begin} = 0.173 → RH_{end} = 0.162. For all figures, Q_f → 0 within 45 s of the last data point.

may be attributed to parameter variability between individual samples, including differences in microchannel and reservoir dimensions, the extent of oxidation and surface roughness of the PDMS reservoirs, and measured *versus* actual values of T and RH directly above the reservoirs. Scatter within measured values of v for a given microchannel/reservoir combination is most likely due to the degree of imprecision associated with the particle tracking methods utilized here, with the uncertainties scaling with the average fluid velocity.

The results shown in Fig. 3*A* indicate that steady flows persist for roughly 18 min before $Q_f \rightarrow 0$, during which time over 50% of the liquid in the inlet reservoir was lost to evaporation. The duration of flow can be extended significantly by the use of several straightforward modifications, including (i) eliminating $Q_{e,in}$ by use of a immiscible liquid cap or a saturated cotton swab placed on top of the inlet meniscus, or (ii) by reducing $Q_{e,in}$ by decreasing D_1 and D_2, such that $D_1 > D_2$, and increasing H to appropriate values as shown in a previous study.[17] Using these techniques, steady flows have been observed to persist for times lasting longer than an hour with little to no variation in the magnitude of v from the initial values in systems with constant T and RH.

For each experiment shown in Fig. 3, substantial flow rates are generated as long as there is a sufficient volume of water in the inlet reservoir ($V_{in} \gg V_{out}$), and flow quickly approaches zero at $t = t_{end}$ as $V_{in} \rightarrow 0$ due to the equalization of the capillary forces in each reservoir ($R_{1,in} \rightarrow R_{1,out}$). A brief decrease in Q_f follows the meniscus rupture from a complete to an incomplete state at a time $t = t_c$, after which Q_f quickly returns to a value close to that seen before rupture. Predicted values of $V_{out} = V_{out}(t)$ reach steady-state within 30 s as long as the initialization value $V_{out}(t = 0)$ is smaller than the steady value, but the magnitude of the outlet initialization volume had no effect on the ultimate steady value of Q_f. The steady values of V_{out} ($t > 0$) yield volumetric flow rates that change very little with time as shown by both the predicted and the measured values in Fig. 3. The small changes observed in Q_f over time may be attributed to (i) increases in $\Delta p_{i,in}$ from evaporation and convection losses acting to decrease Q_f as time increases (since $D_2 > D_1$) and (ii) increases in T (with small changes in RH) acting to increase Q_f as time increases. Therefore, a system with large inlet reservoirs ($\Delta p_{i,in} = 0$) at constant T and RH will exist at a steady-state such that $dV_{out}/dt \approx 0$.

Prediction of steady-state flow rates

When utilizing this passive flow approach for LOC based applications, it is important to understand the dependence of Q_f on the microchannel and reservoir geometries, as well as on the local values of T and RH. To investigate the range of steady-state volumetric flow rates achievable in simple two-reservoir geometries, particle tracking analysis was performed on systems with varying h, w, $D_{1,out}$, $D_{2,out}$, and H_{out} with a large inlet reservoir to ensure that small changes in V_{in} had little effect on Q_f. Values of v were measured for a given microchannel/reservoir system within 1 min after introduction of liquid to the inlet reservoir (3 samples per data point, 8 measurements per sample), with all measurements taken within 4 min such that values of T and RH could be assumed constant. Steady-state values of Q_f were predicted using eqn (1) with $dV/dt = 0$, given laboratory measurements of D_1, D_2, H, T, RH, θ_1, θ_2, and the assumption that $\Delta p_{i,in} = 0$. Fig. 4*A* displays measured and predicted steady-state values of Q_f as a function of the viscous resistance K for microchannels with varying outlet reservoir dimensions. These results highlight the accuracy of the combined geometric/CFD model coupled with eqn (1)–(4) in predicting the dependence of Q_f on the parameters h, w, D_1, D_2, H, T and RH that define a system. The average deviation of the measured values from theoretical predictions for the results shown in Fig. 3*A* was 6.2% with a maximum deviation of 25.3%.

The results shown in Fig. 4*A* illustrate the dependence of Q_f on the dimensions of the outlet reservoir. For example, for a microchannel with $w = 90$ μm, $h = 28$ μm, and $L = 20$ mm

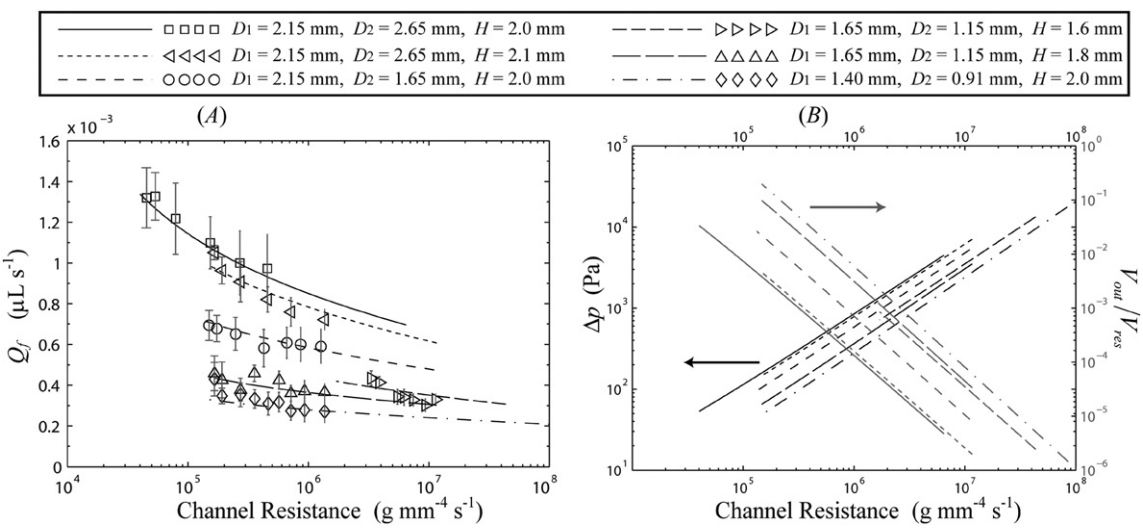

Fig. 4 Experimental and theoretical predictions for: (*A*) volumetric flow rate Q_f *vs.* the viscous channel resistance K for systems with varying microchannel and outlet reservoir dimensions. (*B*) Theoretical predictions for Δp and V_{out}/V_{res} *vs.* K for the values shown in (*A*). Experimental conditions for both figures are (□) $T = 26$ °C, RH = 0.215, (◁) $T = 25.8$ °C, RH = 0.16, (○) $T = 26$ °C, RH = 0.13, (▷) $T = 25$ °C, RH = 0.11, (△) $T = 25.8$ °C, RH = 0.16, (◇) $T = 26.5$ °C, RH = 0.14.

($K = 1.7 \times 10^5$ g mm^{-4} s^{-1}), increasing the overall diameter of the outlet reservoir from (D_1, D_2) = (1.4 mm, 0.91 mm) to (2.15 mm, 2.65 mm) will increase the volumetric flow rate by 224%, from $Q_f = 0.33$ to 1.07 μL s^{-1}. For all of the systems shown in Fig. 4, $V_{out}/V_{res} < 0.1$, such that the wetted sidewall area in the outlet reservoir is predicted to be small and it follows that $Q_{perm} \ll Q_e$. Thus, responses of Q_f to changes in reservoir geometry are mirrored in Q_e. For cylindrical reservoirs with $D_1/H \ll 1$, the volumetric flow rate is predicted to scale with the reservoir dimensions as $Q_f \propto D_1^2$ and $Q_f \propto H^{-1}$. For shallow reservoirs ($D_1/H \gg 1$) the volumetric flow rate will scale as $Q_f \propto D_1$, with the transition between the two scaling rates occurring near $D_1/H \approx 1$. The latter results are consistent with experimental observations of evaporation of liquid from shallow wells.[20,21] Interestingly, a switch of the outlet reservoir diameters D_1 and D_2 at a constant value of H (accomplished by reversing the punch direction in fabrication) leads to only small (<5%) changes in Q_f. Additional discussion of these scaling laws may be found in the ESI†.

Fig. 4*A* also displays the relationship between Q_f and K for a given reservoir, with Q_f increasing slightly with decreasing K. The exact relationship between Q_f and K is complicated, since for a given reservoir decreases in K lead to higher values of V_{out} and thus lower values of Δp, leading to only slight increases in Q_f. This relatively weak dependence will prove beneficial for LOC devices utilizing this flow mechanism, as small deviations in microchannel dimensions from variability in the fabrication process will have a commensurately small effect on Q_f. This effect is not seen in traditional capillary driven LOC devices where the meniscus curvature is restricted according to the geometry of the device and flow rates scale as $Q_f \propto K^{-1}$, as given in eqn (2). Fig.4*B* displays the predicted dependence of the steady values of Δp and V_{out} on K for the values shown in Fig. 4*A* (experimental measurements are omitted for clarity). For channels with large viscous resistances ($K > 10^8$ g mm^{-4} s^{-1}), outlet menisci extended a short distance along the perimeter adjacent to the microchannel outlet. In this large K limit the overall size of the meniscus tends to be of the order of the microchannel size, and discrepancies in Q_f between measurement and prediction were larger than those shown in Fig. 4*A*.

Applications

Due to the ability to provide near-constant continuous flow rates for periods lasting over an hour, this passive pumping system can be applied to nearly all LOC devices that require pressure-driven flow. With precise control of sample-to-sample microchannel and outlet reservoir dimensions, this pumping mechanism has the potential to enhance the repeatability of heterogeneous assays requiring continuous flow for multiple hours, including affinity relationships possessing poor association kinetics or assays based on analytical measurements of live cells. Appropriate design of the inlet reservoirs of such systems would require only pipette delivery of sample volumes $V_o < 10$ μL, eliminating the need for syringe pumps or pressurized vessels.

Because the capillary forces associated with the inlet reservoirs are very small relative to those in the outlet reservoir, a single outlet reservoir can be used to pump fluids from multiple inlet reservoirs with volumetric flow rates from each reservoir dictated by the dimensions of the μFN. A representative example of this reservoir/μFN arrangement can be found in the passive generation of chemical gradients utilizing the techniques displayed by Jeon *et al.*[22] The configuration of a μFN used to passively create varying protein concentrations within a series of 8 outlet channels from two inlet reservoirs is shown in Fig. 5*A*, where the μFN had individual channel dimensions of $w = 24$ μm and $h = 20$ μm connected to an outlet reservoir with $D_1 = 2.15$ mm, $D_2 = 1.65$ mm, and $H = 1.5$ mm. The two inlet reservoirs were charged sequentially with solutions containing 1 μg mL^{-1} and 10 μg mL^{-1} of fluorescently labeled IgG ($V_o = 3.0$ μL), after which capillary filling of the μFN was completed in less than 30 s. Steady flow was maintained for over 75 min ($Q_f = 6.1 \times 10^{-4}$ μL s^{-1}, $K = 1.2 \times 10^6$ g mm^{-4} s^{-1}), where the average fluid velocity along each of the 8 outlet channels was measured to be 158 ± 6 μm s^{-1}. Fluorescence images of the region near the outlet meniscus can be seen in Fig. 5*B* ($t = 60$ min); all 8 channels developed steady fluorescent profiles within 3 min, as shown in Fig. 5*C*. By capping each inlet reservoir with 1.0 μL of heavy mineral oil, the concentrations of the aqueous solutions in each reservoir are maintained over time ($Q_{e,in} = 0$), and the fluorescent intensity profile of the outlet channels at $t = 60$ min remains within 15% of the profile seen at $t = 3$ min. The slight increase in fluorescence intensity is most likely due to the adsorption of fluorescently labeled protein onto the microchannel walls over time. Conversely, if nothing is done to mitigate evaporation from the inlet reservoir the concentrations in each outlet channel increase steadily over time, resulting in nearly a 100% increase in fluorescent intensity within each channel at $t = 30$ min. Because evaporation occurs from all reservoirs in that case, steady flow was only maintained for 35 min.

Suspended or dissolved material within the inlet reservoir is rapidly concentrated in the outlet reservoir in these systems due to the small, ~1 pL, steady-state values of V_{out}. Furthermore, the recirculation profiles present in the outlet reservoir (seen in the supplementary videos†) serve to mix the reservoir contents and help maintain a uniform concentration throughout the solution. This effect is evident in the fluorescence image shown in Fig. 5*B*, where there is a sharp increase in fluorescence intensity between the microchannels and outlet reservoir meniscus. For this case a steady value of $V_{out} = 2.0$ pL is predicted, and after 60 min of flow the material in the outlet reservoir is concentrated by over 3 orders of magnitude above the inlet value. The controlled concentration of confined fluids in the outlet reservoir would prove beneficial to many LOC applications, such as the qualitative detection of analyte *via* heterogeneous immunoassays.

The concentration of material in the outlet reservoir limits the overall flow duration for a given system as solutes crystallize near the outlet meniscus; however, material tends to crystallize in the reservoir at the point farthest from the microchannel outlet, allowing flow to continue at a controlled rate for extended times. The overall duration of flow for a single outlet reservoir is thus limited by both the initial concentrations and the solubility of the solutes placed in the inlet reservoir. This limitation can be alleviated by the use of multiple outlet reservoirs, where multiple reservoirs with small diameters can produce larger steady-state values of V_{out} such that the rate of concentration in each reservoir is minimized and flow can be maintained for longer periods of time. In addition, the use of multiple outlet reservoirs also provides a larger range of Q_f compared to those shown in Fig. 4A,

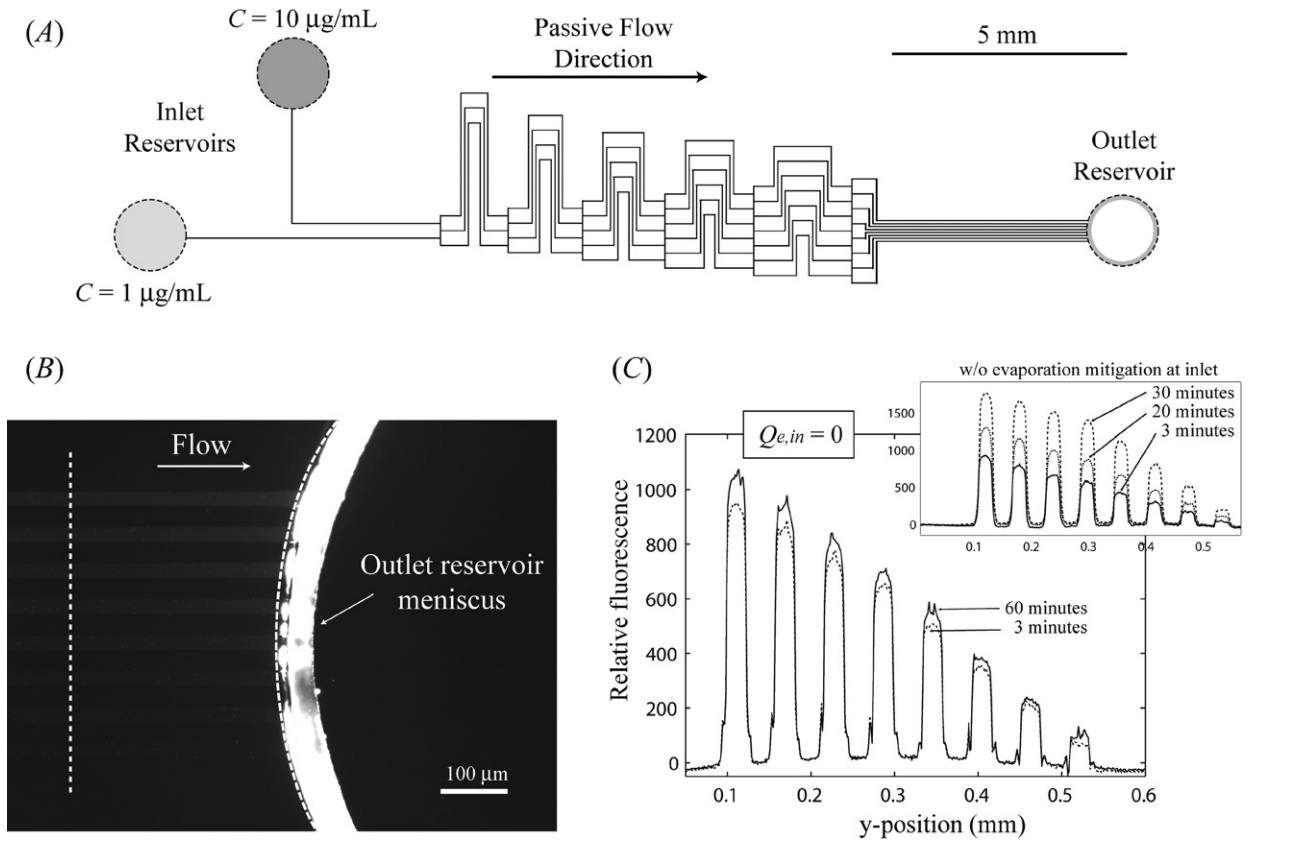

Fig. 5 (*A*) Overall μFN design for the passive generation of chemical gradients in 8 outlet channels from 2 inlet reservoirs. (*B*) Fluorescence intensity ($t = 60$ min) for the 8 outlet channels for the case with the inlet channels containing 10 μg mL^{-1} and 1 μg mL^{-1} of fluorescently labeled IgG, respectively. The position of the incomplete meniscus did not change over time. (C) Relative fluorescence intensity for the 8 outlet channels for 3 and 60 min when the inlet reservoirs were capped with mineral oil. The inset displays the same profile when the inlet reservoirs were open to evaporation.

because volumetric flow rates may be increased (approximately) in proportion to the number of outlet reservoirs. Predicting Q_f in μFNs with N outlet reservoirs involves the solution to $N + 1$ non-linear equations and is beyond the scope of this study.

Materials and methods

Solution

For particle tracking experiments, solutions of fluorescent polystyrene microspheres (Duke Scientific) in nanopure water (Barnstead) were stabilized with tween-20 (Sigma) at a concentration of 1.5×10^{-7} M. The number density of the spheres ranged from 1.3×10^7 to 6.5×10^7 mL^{-1} depending on the height of the microchannel and speed of flow. To create chemical gradients, purified solutions of polyclonal IgG (Invitrogen) were fluorescently labeled with Alexa Fluor 488 protein labeling kit (Invitrogen) and diluted to the proper concentrations in PBS (150 mM NaCl, 50 mM Na_2HPO_4, pH 7.4) along with 1.0 mg mL^{-1} of bovine serum albumin (Sigma), 1.5×10^{-7} M tween-20, and a microsphere density of 1.3×10^6 mL^{-1}. All solutions were aggressively vortexed for 30 s before sample introduction to the inlet reservoir.

Fabrication of channels

Microchannel molds were composed of the negative photoresist Su-8 (Microchem) on polished silicon wafers (University Wafers). Heights of the microchannels were measured with a profilometer and channel widths were measured with a calibrated microscope. Microchannels were created by curing a degassed 1 : 10 curing agent : base mixture of PDMS prepolymer (Sylgard 184, Dow Corning) on the Su-8 molds at 110 °C for 120 min. After curing, conical reservoirs were created using high precision biopsy punches of varying dimension (Technical Innovations). All reservoirs were free of rough edges and burrs, as fluid flow in non-uniform reservoirs was generally unpredictable. The PDMS substrates were then treated in an extraction process to remove unreacted oligomers, and subsequently rinsed with deionized water and gently blown dry with nitrogen.[23] After plasma oxidation at 18 W for 30 s, the PDMS channels were bonded to a cleaned microscope slide. Flow experiments were typically started within 10 min of bonding; however, it is possible to maintain steady flows up to one day after microchannel fabrication. Flow was initiated by the introduction of a liquid volume V_o to the inlet reservoir, and measurements of T and RH were taken approximately 6″ above the sample using a Fluke 971 temperature/humidity meter.

Particle tracking

Immediately after liquid introduction into the inlet reservoir, the glass/PDMS microchannels were placed on an inverted microscope equipped with an epifluorescence attachment (Nikon

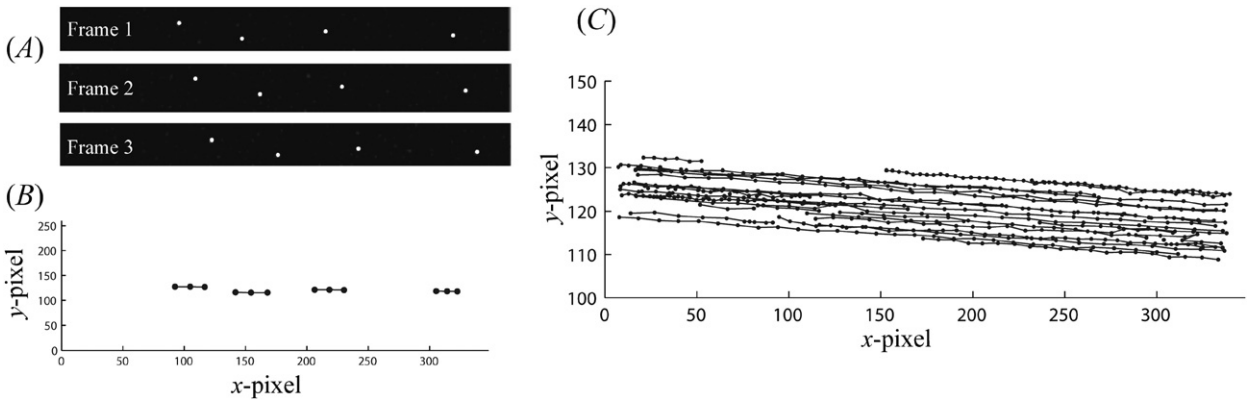

Fig. 6 (*A*) Three consecutive frames (taken at $\Delta t = 30$ ms apart) showing the locations of 4 individual beads after particle location refinement. (*B*) *y*- *vs.* *x*-pixel trajectories linked by individual particles for the positions shown in (*A*). (*C*) Trajectories of 45 particles taken from 100 images in a channel of $h = 5$ μm and $w = 50$ μm flowing at an average linear velocity of $v = 860$ μm s^{-1}.

TE-2000U) fitted with a monochrome CCD camera (Coolsnap fx) using the program Metamorph (Molecular Devices). For particle tracking, images were acquired sequentially at 100× magnification with an exposure time of 5 ms and $\Delta t = 30$ ms between exposures. Particle tracking studies were performed using the methods developed by Crocker and Grier.[24] Near instantaneous measurements of v for unidirectional flow were accomplished by capturing a minimum of 150 sequential images displaying positions of tracer beads. Each image was refined with a bandpass filter to suppress pixel noise, after which the location of individual tracer beads was determined using a minimum intensity threshold. Particle locations were then refined to give estimates of the centroid positions, shown for three images in Fig. 6*A* for 0.5 μm diameter beads flowing in a microchannel of $h = 5$ μm and $w = 50$ μm at an average velocity of $v = 860$ μm s^{-1}. A dataset consisting of the *x*- and *y*-positions of each observation at time t is used with the algorithm developed by Crocker and Grier to link particles into individual trajectories, as shown in Fig. 6*B* for the three images in Fig. 6*A*. Fig. 6*C* displays the linked trajectories of 45 particles taken over 100 consecutive images. After the particle trajectories were calculated, particle velocity vectors were estimated using $v_{\text{particle}} = \Delta x/\Delta t$. Utilizing experimental measurements of w and h, average fluid velocities were then calculated from an average of the top 50 maximum particle velocity ($v_{\max}$) observations along with a relation of v *vs.* $v_{\max}$ acquired from the Boussinesq series solution for viscous flow in a rectangular duct.[25] Due to the small size of the tracer particles and the low Reynolds numbers present in this system, it may be assumed that $\boldsymbol{v}_{\text{particle}} = \boldsymbol{v}_{\text{fluid}}$ for particles in channel locations where the fluid is at a maximum velocity.[26]

The algorithms illustrated in Fig. 6 do not give accurate results if the flow is sufficiently fast and the particle densities are such that there is less than 5 μm between each particle. The CCD camera used in this study was limited to times between consecutive images of $\Delta t = 30$ ms. As a result, accurate measurements were limited to flows of $v < 3.5$ mm s^{-1}. Flow rates exceeding $v > 1$ mm s^{-1} required very dilute particle concentrations such that each image contained less than 5 particles at a given time. For purposes of accuracy, the results of this study were limited to flows such that $v < 2$ mm s^{-1}. The particle tracking algorithms were verified by manual location of individual particle tracks for a stream of images.

Conclusions

In summary, a passive pumping strategy has been demonstrated that provides near-constant flow rates from ~1 μL sample volumes for periods exceeding an hour. The simple system requires only fluid delivery to one or more inlet reservoirs after which steady-state passive flow is spontaneous, driven by a small meniscus existing on the bottom corner region of an outlet reservoir. The modeling approach used in this study has been shown to accurately predict the volumetric flow rate (Q_f) and time to dry out (t_{end}) in μFNs with one outlet reservoir. Because the passive pumping mechanism shown here requires only that the microchannel/reservoir system be sufficiently hydrophilic, these systems can be fabricated from multiple constructs and are not limited to PDMS or glass substrates. Appropriate flow rates for a given μFN are accomplished *via* control over the dimensions of both the microchannels and the outlet reservoirs. The techniques used in this study can be easily integrated to any LOC device utilizing pressure-driven flow.

Acknowledgements

The authors thank Charles Henry and Brian Murphy for their stimulating discussion and help with fluorescent labeling of IgG. This work was supported by NIH grant number EB00726.

References

1 K. Ohno, K. Tachikawa and A. Manz, *Electrophoresis*, 2008, **29**, 4443–4453.
2 S. Pennathur, *Lab Chip*, 2008, **8**, 383–387.
3 A. Nisar, N. AftuIpurkar, B. Mahaisavariya and A. Tuantranont, *Sens. Actuators, B*, 2008, **130**, 917–942.
4 D. C. Duffy, H. L. Gillis, J. Lin, N. F. Sheppard and G. J. Kellogg, *Anal. Chem.*, 1999, **71**, 4669–4678.
5 A. Wixforth, C. Strobl, C. Gauer, A. Toegl, J. Scriba and Z. von Guttenberg, *Anal. Bioanal. Chem.*, 2004, **379**, 982–991.
6 G. Blanco-Gomez, A. Glidle, L. M. Flendrig and J. M. Cooper, *Anal. Chem.*, 2009, **81**, 1365–1370.

7 M. A. Unger, H. P. Chou, T. Thorsen, A. Scherer and S. R. Quake, *Science*, 2000, **288**, 113–116.
8 H. Andersson, W. van der Wijngaart, P. Nilsson, P. Enoksson and G. Stemme, *Sens. Actuators, B*, 2001, **72**, 259–265.
9 D. J. Laser and J. G. Santiago, *J. Micromech. Microeng.*, 2004, **14**, R35–R64.
10 M. Zimmermann, H. Schmid, P. Hunziker and E. Delamarche, *Lab Chip*, 2007, **7**, 119–125.
11 S. Cesaro-Tadic, G. Dernick, D. Juncker, G. Buurman, H. Kropshofer, B. Michel, C. Fattinger and E. Delamarche, *Lab Chip*, 2004, **4**, 563–569.
12 D. Juncker, H. Schmid, U. Drechsler, H. Wolf, M. Wolf, B. Michel, N. de Rooij and E. Delamarche, *Anal. Chem.*, 2002, **74**, 6139–6144.
13 G. M. Walker and D. J. Beebe, *Lab Chip*, 2002, **2**, 131–134.
14 E. Berthier and D. J. Beebe, *Lab Chip*, 2007, **7**, 1475–1478.
15 I. J. Chen, E. C. Eckstein and E. Lindner, *Lab Chip*, 2009, **9**, 107–114.
16 E. Berthier, J. Warrick, H. Yu and D. J. Beebe, *Lab Chip*, 2008, **8**, 852–859.
17 N. S. Lynn, C. S. Henry and D. S. Dandy, *Lab Chip*, 2009, **9**, 1780–1788.
18 E. W. Washburn, *Phys. Rev.*, 1921, **17**, 273–283.
19 W. M. Rohsenow, J. P. Hartnett and Y. I. Cho, *Handbook of Heat Transfer*, McGraw-Hill, New York, 1998.
20 C. T. Chen, F. G. Tseng and C. C. Chieng, *Sens. Actuators, A*, 2006, **130**, 12–19.
21 L. R. van den Doel and L. J. van Vliet, *Appl. Opt.*, 2001, **40**, 4487–4500.
22 N. L. Jeon, S. K. W. Dertinger, D. T. Chiu, I. S. Choi, A. D. Stroock and G. M. Whitesides, *Langmuir*, 2000, **16**, 8311–8316.
23 J. A. Vickers, M. M. Caulum and C. S. Henry, *Anal. Chem.*, 2006, **78**, 7446–7452.
24 J. C. Crocker and D. G. Grier, *J. Colloid Interface Sci.*, 1996, **179**, 298–310.
25 L. A. Belfiore, *Transport Phenomena for Chemical Reactor Design*, Wiley, New York, 2003.
26 M. E. Staben, A. Z. Zinchenko and R. H. Davis, *Phys. Fluids*, 2003, **15**, 1711–1733.